



## Selection rule for the photoinduced phase transition dominated by anisotropy of strain in $\text{Ti}_3\text{O}_5$

Takuo Saiki <sup>1</sup>, Taishi Yoshida,<sup>1</sup> Kaoru Akimoto,<sup>1</sup> Daigo Indo,<sup>2</sup> Mitsutoshi Arizono,<sup>2</sup> Tetsuji Okuda,<sup>2</sup> and Takuro Katsufuji <sup>1,3</sup>

<sup>1</sup>*Department of Physics, Waseda University, Tokyo 169-8555, Japan*

<sup>2</sup>*Graduate School of Science and Engineering, Kagoshima University, Kagoshima 890-0065, Japan*

<sup>3</sup>*Kagami Memorial Research Institute for Materials Science and Technology, Waseda University, Tokyo 169-0051, Japan*



(Received 19 November 2021; revised 1 February 2022; accepted 1 February 2022; published 18 February 2022)

In photoinduced phase transitions, the relationship between the crystal orientation and the direction of the polarization or wave vector of light seems important, but surprisingly, such directional properties in photoinduced phase transitions have not been well studied experimentally.  $\text{Ti}_3\text{O}_5$  exhibits a structural phase transition involving the anisotropic migration of Ti and O ions, and its nanocrystals exhibit a persistent photoinduced phase transition. We found that a photoinduced phase transition occurs even in a single crystal of this compound, but it significantly depends on the orientation of the plane on which the light is irradiated. Such a selection rule for photoinduced phase transitions is dominated by the anisotropy of the strain associated with the phase transition.

DOI: [10.1103/PhysRevB.105.075134](https://doi.org/10.1103/PhysRevB.105.075134)

### I. INTRODUCTION

Photoinduced phase transitions are phenomena in which the application of a laser pulse to a material induces phase transition in the material. It has been observed in various types of phase transition, for example, the Mott transition [1–10], charge ordering [11–15], orbital ordering [16,17], spin-crossover transition [18,19], and charge density wave transition [20]. These phase transitions are mostly categorized into electronic phase transitions, in which the driving force of the phase transitions is electronic, although it is often accompanied by a small lattice distortion associated with the change in electronic structure. Regarding such phase transitions induced by a laser pulse, since light has its own directions of the polarization and wave vector, how the photoinduced phase transitions depend on these directions with respect to the crystal orientation is an interesting issue. However, the intrinsic dependence of photoinduced phase transitions on the directional properties of light has hardly been studied thus far, except for the apparent dependence on the polarization direction arising from the different absorption coefficient of the material.

Research on photoinduced phase transitions accompanied by a migration of atoms in the crystals has been conducted much less than that on electronic phase transitions, and their study on  $\text{Ti}_3\text{O}_5$  is one of the rare examples.  $\text{Ti}_3\text{O}_5$  [21–31] has Ti ions with an average valence of 3.3+, that is, there are nominally two  $\text{Ti}^{3+}$  ( $3d^1$ ) ions and one  $\text{Ti}^{4+}$  ( $3d^0$ ) ion, and it exhibits successive structural phase transitions with increasing temperature from the monoclinic  $\beta$  phase [low-temperature (LT) phase] to the monoclinic  $\lambda$  phase [intermediate-temperature (IT) phase] at  $\sim 460$  K and from the  $\lambda$  phase to the orthorhombic  $\alpha$  phase (high-temperature phase) at  $\sim 500$  K. The  $\beta$  phase (LT phase) is characterized

by the  $\text{Ti}^{3+}$ - $\text{Ti}^{3+}$  dimer along the  $c$  axis and that along the  $a$  axis, but the dimer along the  $c$  axis disappears in the  $\lambda$  phase (IT phase) because of the migration of Ti and O ions with the phase transition, as shown in Figs. 1(a) and 1(b). Various physical properties drastically change with this  $\beta \rightarrow \lambda$  phase transition. Furthermore, the transition temperatures decrease with Al doping into the Ti site of  $\text{Ti}_3\text{O}_5$  and the phase at room temperature changes from  $\beta$  to  $\lambda$  and  $\alpha$  for  $\text{Ti}_{3-x}\text{Al}_x\text{O}_5$  with increasing  $x$  [29].

Photoinduced phase transitions have been observed in nanocrystals of  $\text{Ti}_3\text{O}_5$  [25], where the  $\beta$  (LT) and  $\lambda$  (IT) phases coexist at room temperature. When a nanosecond laser pulse is applied to these nanocrystals, a permanent change from the  $\beta$  phase to the  $\lambda$  phase or from the  $\lambda$  phase to the  $\beta$  phase occurs depending on the intensity of the laser pulse. Recently, the photoinduced phase transition of the  $\text{Ti}_3\text{O}_5$  nanocrystals has been studied by time-resolved x-ray diffraction [31], and it has been clarified that the change in lattice structure from the  $\beta$  phase to the  $\lambda$  phase is associated with the propagation of strain wave, whose timescale is on the order of several picoseconds.

One of the unclarified issues on the photoinduced phase transitions of  $\text{Ti}_3\text{O}_5$  is the role of nanocrystals. It seems likely that the  $\lambda$  (IT) phase is more stabilized compared with the  $\beta$  (LT) phase in nanocrystals and as a result, the two phases coexist at room temperature. However, it is not clear how the size of the crystal affects the processes of photoinduced phase transitions. In addition, we consider that this compound is a good system for studying the possible dependence of photoinduced phase transitions on the direction of the polarization or wave vector of light with respect to the orientation of the crystal, since the phase transitions involve the migration of atoms with anisotropy. In this study, we performed

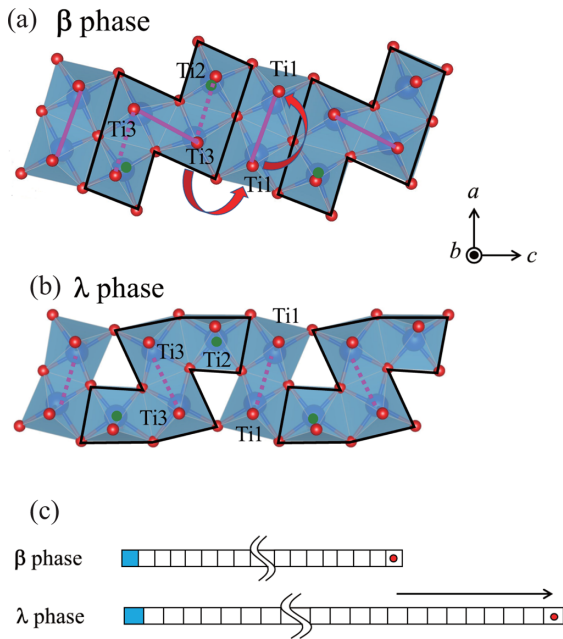


FIG. 1. (a), (b) Crystal structure of  $\text{Ti}_3\text{O}_5$  in the (a)  $\beta$  phase (low-temperature phase) and (b)  $\lambda$  phase (intermediate-temperature phase) drawn by VESTA [32]. The arrows in (b) illustrate the excitation that contributes to the peaks in optical conductivity (see text). (c) Schematic illustration of the strain associated with the phase transition from the  $\beta$  phase to the  $\lambda$  phase caused by the accumulation of a change in the lattice constant of the unit cell.

time-resolved pump-probe reflectivity measurements of a  $\text{Ti}_3\text{O}_5$  ( $\beta$  phase) single crystal, and we found that a photoinduced phase transition is severely affected by the orientation of the surface of the crystal on which the laser pulse is irradiated, and this selection rule is dominated by the anisotropy in the macroscopic strain of the material.

## II. EXPERIMENT

The single crystals used in this study were grown by the floating-zone method as described in Ref. [29]. The crystalline axes of the grown crystals were determined by the Laue method. We found that  $\text{Ti}_3\text{O}_5$  is easily cleaved along the surface containing the  $c$  axis; thus, we mainly used the cleaved surfaces along the  $ac$  or  $bc$  plane, whereas the surface along the  $ab$  plane was polished with alumina powder. The effect of polishing on the photoinduced phenomena is discussed in Appendix D. For  $\text{Ti}_{2.75}\text{Al}_{0.25}\text{O}_5$ , the polished surfaces were used for all the planes. Reflectivity measurements at room temperature were performed between 0.08 and 0.8 eV using an FTIR spectrometer and between 0.6 and 5.0 eV using a grating spectrometer. Pump-probe reflectivity measurements were performed using a Ti:sapphire regenerative amplified laser (a pulse width of 130 fs, a repetition rate of 1 kHz, and a wavelength of 795 nm). A laser pulse was divided into a pump pulse and a probe pulse. The pump pulse with a power density of  $<33$  mJ/cm<sup>2</sup> was applied to the sample surface. The probe pulse, which was broadened in frequency between 0.8 and 3.0 eV by self-phase modulation, was applied to the sample surface with various time delays. The reflected light of

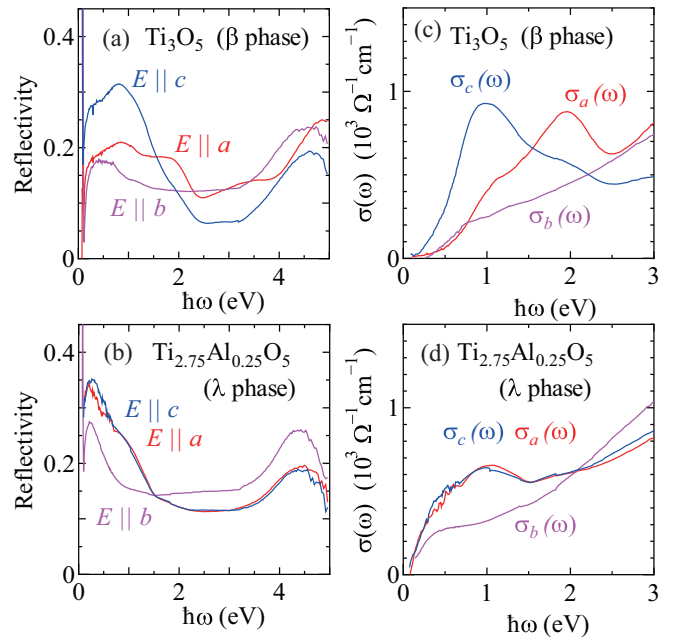


FIG. 2. (a), (b) Reflectivity spectra at room temperature with  $E \parallel a$ ,  $b$ , and  $c$  for (a)  $\text{Ti}_3\text{O}_5$  in the  $\beta$  phase and (b)  $\text{Ti}_{2.75}\text{Al}_{0.25}\text{O}_5$  in the  $\lambda$  phase. (c), (d) Optical conductivity spectra derived from the reflectivity spectra in (a) and (b) for (c)  $\text{Ti}_3\text{O}_5$  in the  $\beta$  phase and (d)  $\text{Ti}_{2.75}\text{Al}_{0.25}\text{O}_5$  in the  $\lambda$  phase.

the probe pulse was monochromated and detected using a Si photodiode.

## III. OPTICAL REFLECTIVITY AND CONDUCTIVITY SPECTRA

Regarding the information necessary to analyze the photoinduced spectra, we first measured the reflectivity spectra of  $\text{Ti}_3\text{O}_5$  as well as  $\text{Ti}_{2.75}\text{Al}_{0.25}\text{O}_5$ , which is in the  $\lambda$  phase at room temperature. Figures 2(a) and 2(b) show the optical reflectivity spectra with the polarization along the  $a$ ,  $b$ , and  $c$  axes at room temperature for (a)  $\text{Ti}_3\text{O}_5$  ( $\beta$  phase) and (b)  $\text{Ti}_{2.75}\text{Al}_{0.25}\text{O}_5$  ( $\lambda$  phase) below 5 eV. Figures 2(c) and 2(d) show the optical conductivity spectra below 3 eV obtained by the Kramers-Kronig transformation of the reflectivity spectra shown in Figs. 2(a) and 2(b). For both compounds, the optical conductivity spectra with  $E \parallel b$  [ $\sigma_b(\omega)$ ] do not show a significant structure below 3 eV. For  $\text{Ti}_3\text{O}_5$ , the optical conductivity spectrum with  $E \parallel c$  [ $\sigma_c(\omega)$ ] has a peak at  $\sim 1$  eV and a small shoulder at  $\sim 2$  eV, whereas that with  $E \parallel a$  [ $\sigma_a(\omega)$ ] has a peak at  $\sim 2$  eV and a small shoulder at  $\sim 1$  eV. These spectra are almost consistent with those obtained by theoretical calculation [31]. On the basis of comparison between the calculated and measured spectra, the peak at 1 eV for  $\sigma_c(\omega)$  can be assigned to the excitation of the  $d$  electron in the bonding state of the Ti dimer along the  $c$  axis to the antibonding state of the Ti dimer along the  $a$  axis, and the peak at 2 eV for  $\sigma_a(\omega)$  can be assigned to the excitation of the  $d$  electron in the bonding state of the Ti dimer along the  $a$  axis to the antibonding state of the same dimer [25,27], as indicated by arrows in Fig. 1(a).

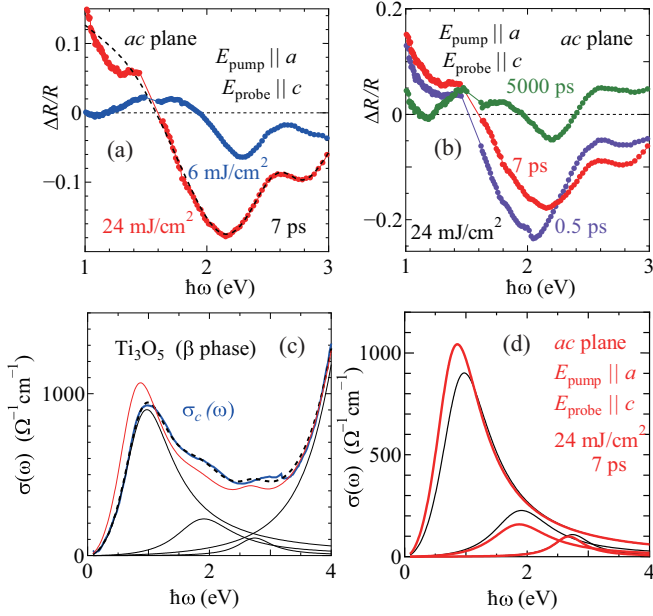


FIG. 3. (a), (b) Photoinduced changes in the reflectivity spectra  $\Delta R/R$  on the  $ac$  plane with  $E_{\text{pump}} \parallel a$  and  $E_{\text{probe}} \parallel c$  at (a)  $t = 7$  ps after a pump pulse with a power density of  $p = 6$  or  $24$   $\text{mJ}/\text{cm}^2$  is applied and (b)  $t = 0.5, 7,$  and  $5000$  ps after a pump pulse with  $p = 24$   $\text{mJ}/\text{cm}^2$  is applied. The dashed line in (a) is a fitting curve (see text). (c) Decomposition of the optical conductivity spectrum of  $\text{Ti}_3\text{O}_5$  along the  $c$  axis into four Lorentz functions. The dashed line is the sum of the Lorentz functions, and the red solid line is the sum of the Lorentz functions with shifted parameters for the photoinduced spectrum in (d). (d) Three Lorentz functions for the optical conductivity spectrum along the  $c$  axis before the application of a pump pulse (thin black lines) and  $7$  ps after a pump pulse of  $p = 24$   $\text{mJ}/\text{cm}^2$  is applied (thick red lines).

On the other hand, the optical conductivity spectra for  $\text{Ti}_{2.75}\text{Al}_{0.25}\text{O}_5$  in the  $\lambda$  phase have little anisotropy between  $\sigma_a(\omega)$  and  $\sigma_c(\omega)$  below  $\hbar\omega < 3$  eV. These spectra are qualitatively consistent with the calculated optical conductivity spectra for the  $\lambda$  phase [31]. This result indicates that the Ti-Ti dimer in the  $\lambda$  phase, which seemingly exists along the  $a$  axis in terms of the crystal structure [dashed lines in Fig. 1(b)], affects the electronic structure much less significantly than the dimer in the  $\beta$  phase. (Reflectivity and optical conductivity spectra of  $\text{Ti}_3\text{O}_5$  at high temperatures, which is possibly in the  $\lambda$  phase, are shown and discussed in Appendix E.)

#### IV. PHOTOINDUCED REFLECTIVITY SPECTRA

Let us see the photoinduced changes in reflectivity spectra. Figure 3(a) shows the photoinduced spectra  $\Delta R/R$  at  $t = 7$  ps after a pump pulse with a power density of  $p = 6$  or  $24$   $\text{mJ}/\text{cm}^2$  is applied to a cleaved surface along the  $ac$  plane of  $\text{Ti}_3\text{O}_5$  with the polarization of a pump pulse along the  $a$  axis and a probe pulse along the  $c$  axis ( $E_{\text{pump}} \parallel a$  and  $E_{\text{probe}} \parallel c$ ). The wavelength of the pump pulse (795 nm) corresponds to  $\hbar\omega = 1.56$  eV, and it is approximately located at the crossing point of  $\sigma_a(\omega)$  having a peak at  $\sim 2$  eV and  $\sigma_c(\omega)$  having a peak at  $\sim 1$  eV. Figure 3(b) shows the photoinduced  $\Delta R/R$  spectra on the same surface with the same polarizations at

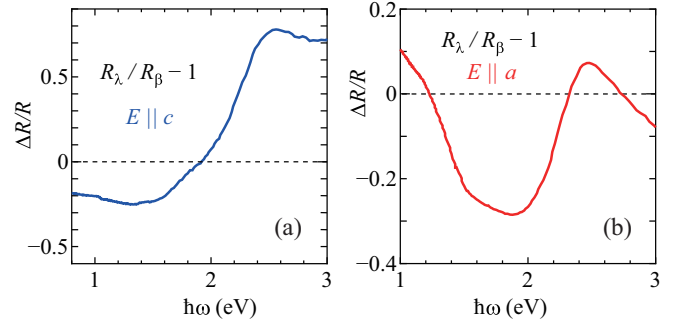


FIG. 4. (a), (b) Difference between the reflectivity spectra for  $\text{Ti}_{2.75}\text{Al}_{0.25}\text{O}_5$  in the  $\lambda$  phase and that for  $\text{Ti}_3\text{O}_5$  in the  $\beta$  phase with (a)  $E \parallel c$  and (b)  $E \parallel a$ .

$t = 0.5$  ps,  $7$  ps, and  $5000$  ps for  $p = 24$   $\text{mJ}/\text{cm}^2$ . In both series of the data, large photoinduced changes are observed. For comparison, the difference between the reflectivity spectrum with  $E \parallel c$  for  $\text{Ti}_{2.75}\text{Al}_{0.25}\text{O}_5$  in the  $\lambda$  phase and that for  $\text{Ti}_3\text{O}_5$  in the  $\beta$  phase is shown in Fig. 4(a). Note that the negative value in the difference spectrum around  $\sim 1$  eV is due to the fact that the peak at  $\sim 1.0$  eV in the  $\sigma_c(\omega)$  spectrum of the  $\beta$  phase [Fig. 2(c)] is suppressed in the  $\lambda$  phase. As can be seen, the photoinduced changes in the reflectivity spectrum shown in Figs. 3(a) and 3(b) are discernibly different from the difference in the reflectivity spectra between the  $\lambda$  (IT) and  $\beta$  (LT) phases shown in Fig. 4(a). Thereby, we can conclude that the photoinduced changes shown in Figs. 3(a) and 3(b) are not caused by the phase transition from the  $\beta$  phase to the  $\lambda$  phase. To clarify what causes the photoinduced spectral change shown in Figs. 3(a) and 3(b), we carried the following procedure: First, the optical conductivity spectrum for  $\text{Ti}_3\text{O}_5$  with  $E \parallel c$  below  $5$  eV shown in Fig. 2(c) was fitted by four Lorentz functions,

$$\sigma(\omega) = \omega^2 \sum_i \frac{C_i \gamma_i}{(\omega^2 - \omega_i^2)^2 + \gamma_i^2 \omega^2}, \quad (1)$$

as shown in Fig. 3(c). Then, the parameters of each Lorentz function (the peak frequency  $\omega_i$ , the width  $\gamma_i$ , and the spectral weight  $S_i$ ) were shifted and the photoinduced spectral change was fitted by the difference between the reflectivity spectrum calculated with the shifted parameters and that with the original parameters, using the following formula of reflectivity:

$$\varepsilon(\omega) = \sum_i \frac{S_i}{\omega^2 - \omega_i^2 - i\gamma_i\omega} + \varepsilon_\infty, \quad (2)$$

$$R(\omega) = \left| \frac{\sqrt{\varepsilon(\omega)} - 1}{\sqrt{\varepsilon(\omega)} + 1} \right|^2. \quad (3)$$

We found that the photoinduced  $\Delta R/R$  spectra can be fitted, as shown by a dashed line in Fig. 3(a), by changing the parameters of three Lorentz functions with the peaks at  $\hbar\omega_0 = 1.0, 1.9,$  and  $2.7$  eV, as shown Fig. 3(d). The parameters obtained by the fitting are shown in Table I of Appendix A. The change in the parameters is such that the peak frequency is shifted to lower values for all of the three peaks, and the spectral weight for the peak at  $\hbar\omega_0 = 1.9$  eV decreases, but that for the peak at  $\hbar\omega_0 = 1.0$  eV increases. The sum of these Lorentz functions with the shifted parameters is shown by the red

line in Fig. 3(c). Such a shift of the spectral weight to lower frequencies is typically observed when the temperature of the sample is increased. Therefore, we conclude that when a pump pulse is applied onto the  $ac$  plane, the temperature of the sample increases, which results in a large photoinduced change in the spectrum. Nevertheless, the sample does not undergo transition into the  $\lambda$  phase but remains in the original  $\beta$  phase.

One of the possible reasons why the application of a pump pulse does not induce a phase transition in this case is the change in lattice constants associated with the transition from the  $\beta$  phase to the  $\lambda$  phase. Among the three lattice constants,  $a$ ,  $b$ , and  $c$ , only  $c$  increases by  $\sim 6\%$  with the phase transition, whereas  $a$  and  $b$  change by much less than  $1\%$  [24]. Therefore, if a pump pulse with a diameter of  $\sim 1$  mm is irradiated onto the  $ac$  plane and causes a transition from the  $\beta$  phase to the  $\lambda$  phase, a circle with a diameter of 1 mm on the sample surface should be expanded by  $\sim 6\%$ , corresponding to  $\sim 60$   $\mu\text{m}$ , in the  $c$  direction. This means that the atoms in the circle have to move at a similar length. Since the speed of the motion of atoms in the crystal is typically less than its sound velocity, which is usually several  $10^3$  m/s, it takes  $\sim 10^{-8}$  s for a 1-mm-diameter part to expand, which is much longer than the timescale of the pump-probe measurement. Therefore, such lattice expansion does not occur and the lattice constant remains smaller than the value expected for the  $\lambda$  phase, resulting in a large strain that can disturb the phase transition.

The consideration above suggests that if a pump pulse is applied onto the  $ab$  plane, the irradiated part of the crystal is  $\sim 100$  nm thick in the  $c$  direction, which is dominated by the penetration depth of the light with the wavelength of 795 nm; accordingly, the expansion of the  $c$  axis associated with the transition from the  $\beta$  phase to the  $\lambda$  phase will not cause a significant strain (see the illustration at the center of Fig. 6). Figure 5(a) shows the photoinduced change in the reflectivity spectra  $\Delta R/R$  at  $t = 7$  ps with  $p = 6$  or  $33$   $\text{mJ}/\text{cm}^2$  along the  $ab$  plane of  $\text{Ti}_3\text{O}_5$  with  $E_{\text{pump}} \parallel a$  and  $E_{\text{probe}} \parallel a$ . One of the differences between  $\Delta R/R$  with  $p = 6$   $\text{mJ}/\text{cm}^2$  and that with  $33$   $\text{mJ}/\text{cm}^2$  is the position of the minimum in the  $\Delta R/R$  spectrum, which shifts from  $\sim 2.0$  eV to  $\sim 1.8$  eV with increasing power density  $p$ , as shown by arrows in Fig. 5(a). Figure 5(b) shows the photoinduced change in the reflectivity spectra  $\Delta R/R$  on the same surface with the same polarizations at  $t = 0.5, 7$ , and  $5000$  ps for  $p = 33$   $\text{mJ}/\text{cm}^2$ . As can be seen, the  $\Delta R/R$  spectrum barely changes with  $t$  from  $0.5$  to  $7$  ps. The  $t$  dependence of  $\Delta R/R$  for various ranges of  $t$  is discussed in detail in Appendix B and Fig. 7. The difference between the reflectivity spectrum with  $E \parallel a$  for  $\text{Ti}_{2.75}\text{Al}_{0.25}\text{O}_5$  in the  $\lambda$  phase and that for  $\text{Ti}_3\text{O}_5$  in the  $\beta$  phase is shown in Fig. 4(b). The photoinduced  $\Delta R/R$  spectra with  $p = 33$   $\text{mJ}/\text{cm}^2$  shown in Figs. 5(a) and 5(b) are similar to the difference spectrum shown in Fig. 4(b), suggesting that a photoinduced phase transition occurs in this case.

The photoinduced  $\Delta R/R$  spectra along the  $ab$  plane were analyzed by the same procedure as that for the spectra along the  $ac$  plane shown in Fig. 3. Namely, the optical conductivity spectrum for  $\text{Ti}_3\text{O}_5$  with  $E \parallel a$  below  $5$  eV was fitted by four Lorentz functions as shown in Fig. 5(c), and the photoinduced reflectivity spectra were fitted by the

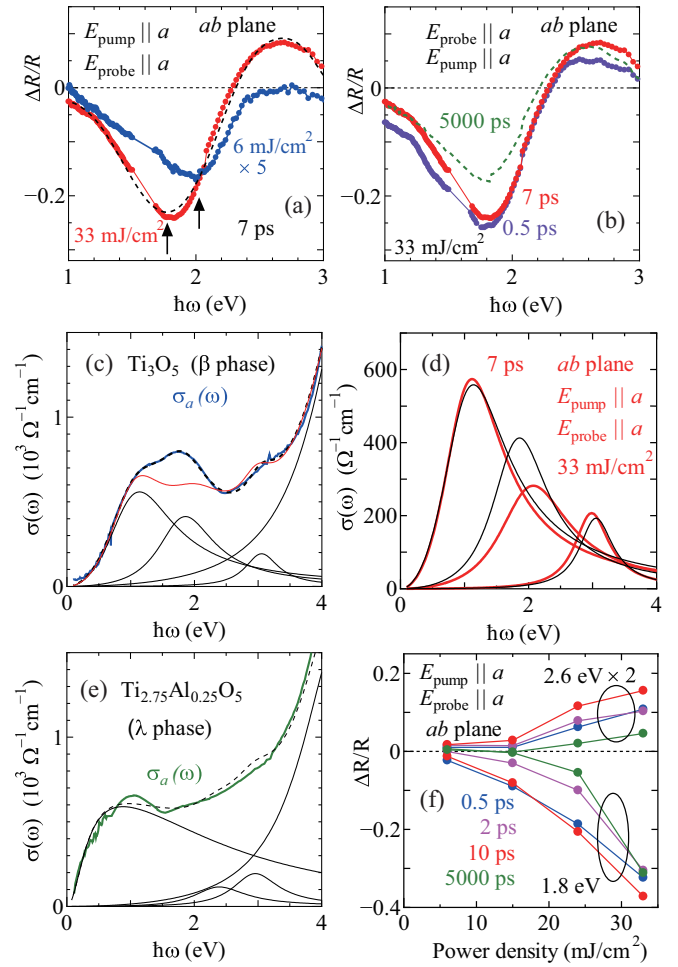


FIG. 5. (a), (b) Photoinduced changes in the reflectivity spectra  $\Delta R/R$  on the  $ab$  plane with  $E_{\text{pump}} \parallel a$  and  $E_{\text{probe}} \parallel a$  at (a)  $t = 7$  ps after a pump pulse with a power density of  $p = 6$  or  $33$   $\text{mJ}/\text{cm}^2$  is applied and (b) at  $t = 0.5, 7$ , and  $5000$  ps after a pump pulse with  $p = 33$   $\text{mJ}/\text{cm}^2$  is applied. The dashed line in (a) is a fitting curve (see text). (c) Decomposition of the optical conductivity spectrum of  $\text{Ti}_3\text{O}_5$  along the  $a$  axis into four Lorentz functions. The dashed line is the sum of the Lorentz functions, and the red solid line is the sum of the Lorentz functions with shifted parameters for the photoinduced spectrum in (d). (d) Three Lorentz functions for the optical conductivity spectrum along the  $a$  axis on the  $ab$  plane before the application of a pump pulse (thin black lines) and  $7$  ps after a pump pulse of  $33$   $\text{mJ}/\text{cm}^2$  (thick red lines) is applied. (e) Decomposition of the optical conductivity spectrum of  $\text{Ti}_{2.75}\text{Al}_{0.25}\text{O}_5$  along the  $a$  axis into four Lorentz functions. (f) The size of the photoinduced reflectivity change  $\Delta R/R$  at  $\hbar\omega = 1.8$  eV and  $2.6$  eV at various values of  $t$  as a function of the power density of the pump pulse  $p$ .

difference between the reflectivity spectrum with the shifted parameters and that with the original parameters, as shown by a dashed line in Fig. 5(a). Figure 5(d) shows the three Lorentz functions at  $\hbar\omega = 1.1, 1.9$ , and  $3.1$  eV before (with original parameters) and after (with shifted parameters) the photoirradiation at  $p = 33$   $\text{mJ}/\text{cm}^2$ . The sum of the Lorentz functions with the shifted parameters is shown by the red line in Fig. 5(c). As can be seen, the intensity of the peak in  $\sigma(\omega)$  at  $\sim 2.0$  eV is substantially suppressed, resulting in the dip in the  $\Delta R/R$  spectrum at  $1.8$  eV. Note that the peak



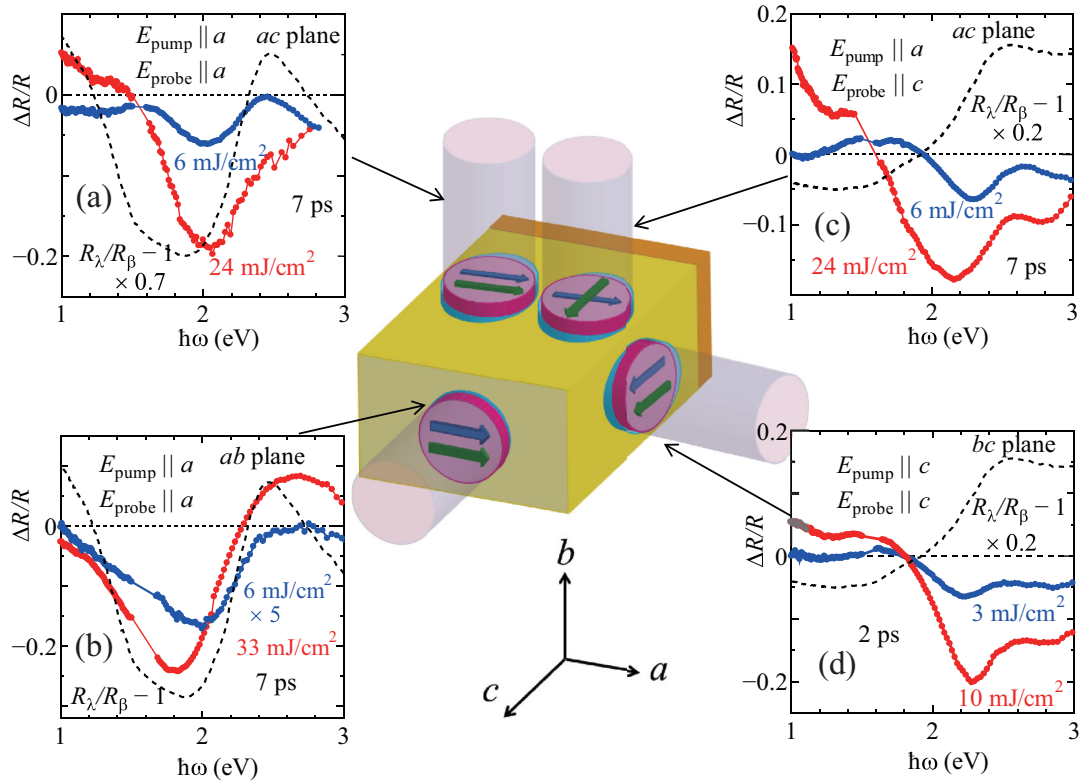


FIG. 6. Photoinduced changes in the reflectivity spectra  $\Delta R/R$  at  $t = 7$  ps for (a)  $E_{\text{pump}} \parallel a$  and  $E_{\text{probe}} \parallel a$  with  $p = 6$  and  $24 \text{ mJ/cm}^2$  on the  $ac$  plane, (b)  $E_{\text{pump}} \parallel a$  and  $E_{\text{probe}} \parallel a$  with  $p = 6$  and  $33 \text{ mJ/cm}^2$  on the  $ab$  plane, (c)  $E_{\text{pump}} \parallel a$  and  $E_{\text{probe}} \parallel c$  with  $p = 6$  and  $24 \text{ mJ/cm}^2$  on the  $ac$  plane, and (d)  $E_{\text{pump}} \parallel c$  and  $E_{\text{probe}} \parallel c$  with  $p = 3$  and  $10 \text{ mJ/cm}^2$  on the  $bc$  plane ( $t = 2$  ps in this case). The dashed line in each figure shows the difference between the reflectivity spectrum of  $\text{Ti}_{2.75}\text{Al}_{0.25}\text{O}_5$  in the  $\lambda$  phase and that of  $\text{Ti}_3\text{O}_3$  in the  $\beta$  phase with a corresponding polarization of the probe pulse. The illustration at the center shows the directions of the crystal axes, the polarization directions of the pump (blue arrows) and probe (green arrows) pulses, the configuration of the laser spot of the pump pulse (magenta circles), and the expansion of the crystal with the  $\beta \rightarrow \lambda$  phase transition (cyan circles and an orange cuboid).

at  $\sim 2.0$  eV in the  $\sigma_a(\omega)$  spectra corresponds to the excitation of the  $d$  electron in the bonding state of the Ti dimer along the  $a$  axis to the antibonding state of the same dimer [an arrow in Fig. 1(a)] and is almost absent in the  $\lambda$  phase, as shown in Fig. 5(e). Therefore, the suppression of this peak by photoirradiation is the direct evidence that the photoinduced transition from the  $\beta$  phase to the  $\lambda$  phase occurs in this configuration.

Figure 5(f) shows the dependence of  $\Delta R/R$  with  $\hbar\omega = 1.8$  eV and 2.6 eV at various values of  $t$  on the power density of the pump pulse  $p$ . As can be seen,  $|\Delta R/R|$  increases superlinearly with  $p$  at any values of  $\hbar\omega$  and  $t$ , characteristic behavior of the photoinduced phase transition [11,33–36].

Note that when a laser pulse is applied to the  $ab$  plane, a change in the reflectivity  $\Delta R/R$  corresponding to the phase transition occurs within 0.5 ps after the photoirradiation, as shown in Fig. 5(b). However, this timescale is shorter than that of the migration of atoms. This indicates that the electronic structure characteristic of the  $\beta$  phase, the  $\text{Ti}^{3+}\text{-Ti}^{3+}$  bonds along the  $c$  or  $a$  axis, disappears immediately after the application of a laser pulse; subsequently, the Ti and O atoms migrate so that the system is in the  $\lambda$  phase.

To further confirm the importance of the direction of the photoirradiated plane, we performed a pump-probe measurement with the same polarization directions of the pump and

probe pulse ( $E_{\text{pump}} \parallel a$  and  $E_{\text{probe}} \parallel a$ ) but on a different plane, the  $ac$  plane. The photoinduced  $\Delta R/R$  spectra with these plane and polarization directions at 7 ps are shown in Fig. 6(a), together with Fig. 6(b) with  $\Delta R/R$  with  $E_{\text{pump}} \parallel a$  and  $E_{\text{probe}} \parallel a$  on the  $ab$  plane (shown in Fig. 5), Fig. 6(c) with  $E_{\text{pump}} \parallel a$  and  $E_{\text{probe}} \parallel c$  on the  $ac$  plane (shown in Fig. 3), and Fig. 6(d) with  $E_{\text{pump}} \parallel c$  and  $E_{\text{probe}} \parallel c$  on the  $bc$  plane. It should be emphasized that in all the configurations in Fig. 6 except for (d), the polarization of the pump pulse is along the  $a$  axis and thus, its penetration depth is the same even if the direction of the surface onto which the pump pulse is irradiated is different. The  $\Delta R/R$  spectrum in Fig. 6(a) with  $p = 24 \text{ mJ/cm}^2$  appears to be similar to that in Fig. 6(b) with  $p = 33 \text{ mJ/cm}^2$ , but the position of the minimum in  $\Delta R/R$  of Fig. 6(a) ( $\sim 2.0$  eV) is higher than that of Fig. 6(b) ( $\sim 1.8$  eV). Indeed, the  $\Delta R/R$  spectrum with  $p = 24 \text{ mJ/cm}^2$  in Fig. 6(a) does not coincide with the difference between the reflectivity spectrum of the  $\lambda$  phase and that of the  $\beta$  phase shown by the dashed line in the same figure. We confirmed that this spectral change in Fig. 6(a) can also be explained by the shift of the peak frequency  $\omega_i$  to lower values, as is the case for Fig. 6(c), with  $E_{\text{pump}} \parallel a$  and  $E_{\text{probe}} \parallel c$  on the  $ac$  plane (Appendix C). The comparison between Fig. 6(a) and Fig. 6(b) indicates that the photoinduced phase transition occurs on the  $ab$  plane but not on the  $ac$  plane.

## V. DISCUSSION

Let us discuss how the process of the photoinduced phase transition proceeds in  $\text{Ti}_3\text{O}_5$  after the photoirradiation to the sample surface. (1) First, the electronic excitation occurs on a timescale of 10 fs, which is dominated by the transfer integral or band gap of the material ( $\sim 1$  eV). (2) Then, the Ti-Ti dimer in a spin singlet is suppressed on a timescale shorter than 1 ps. (3) Subsequently, the energy is transferred in several picoseconds to the lattice, resulting in the increase in lattice temperature. The local atomic migration associated with the transition from the  $\beta$  to  $\lambda$  phase occurs also on this timescale [31]. (4) Finally, the accumulation of the local migration of atoms in many unit cells results in a macroscopic elastic deformation of the crystal, as illustrated in Fig. 1(c).

However, if an irradiated part of the sample has a macroscopic length along the direction where the lattice parameter is expected to change significantly with a phase transition, process (4) takes much longer time than the timescales for processes (1)–(3), which in principle does not occur. Such absence of macroscopic deformation to the equilibrium state acts as a strain to stabilize the ground state ( $\beta$  phase) compared with the photoinduced state ( $\lambda$  phase). This will disturb processes (2) and (3) and prevent the photoinduced phase transition when the laser pulse is applied to the plane containing the  $c$  axis.

We consider that such an effect arising from differences in the timescales of dynamics is analogous to the Frank-Condon principle, which is a rule in general when the electronic excitation in the optical process is coupled to the vibronic excitation [37]. In a process dominated by this principle, since the electronic excitation occurs almost instantaneously compared with the timescale of the vibronic atomic motion and the equilibrium position of atoms in the electronically excited state is different from that in the ground state, the electronic excitation inevitably induces vibronic excitations. In the present case, the electronic excitation and atomic migration can occur almost instantaneously compared with the timescale of the macroscopic deformation associated with the phase transition. This can disturb the photoinduced phase transition, resulting in the “selection rule” of photoinduced phase transitions, which is determined by the size of the irradiated part of the crystal and the direction of the crystal along which the lattice constant significantly changes.

It is known that physics similar to that discussed above (that the crystal expands only to a limited extent along the surface) gives rise to a longitudinal acoustic mode propagating perpendicular to the sample surface when a pump pulse is applied and such a strain wave can cause a photoinduced phase transition [38–40]. Nevertheless, a selection rule of photoinduced phase transitions caused by the anisotropy in the deformation of the crystal has not been investigated or discussed so far. Note also that the present result clarifies the important role of the size of the crystal in photoinduced phase transitions. Namely, for nanocrystals with a size of  $\sim 100$  nm, whichever direction the laser pulse is applied, a large change in  $c$  lattice constant does not induce a strain that possibly disturbs the photoinduced phase transitions.

## VI. SUMMARY

We performed a pump-probe reflectivity measurement for a single crystal of  $\text{Ti}_3\text{O}_5$ , whose nanocrystals are known to exhibit a photoinduced phase transition. A large change in the reflectivity with a photoirradiation was observed in various configurations of the polarization directions and on various sample surfaces for the single crystal of  $\text{Ti}_3\text{O}_5$ . However, by comparing the photoinduced change in the reflectivity spectrum with the difference between the reflectivity in the low-temperature ( $\beta$  phase) and that in the higher-temperature ( $\lambda$ ) phase, we found that a photoinduced phase transition from the  $\beta$  phase to the  $\lambda$  phase occurs only when the pump pulse is applied on the  $ab$  plane. Based on the fact that only the  $c$  lattice constant substantially changes with the phase transition, such a selection rule of the photoinduced phase transition is likely to be dominated by the anisotropy of the strain with the phase transition and the shape of the photoirradiated part of the crystal, which is longer along the surface plane but is much smaller perpendicular to it.

## ACKNOWLEDGMENTS

We thank T. Mizokawa for fruitful discussions. This work was supported by JSPS KAKENHI Grant No. 19H01853. The experiment was partly carried out at the Joint Research Center for Environmentally Conscious Technologies in Materials Science (Grant No. PMXP0618217637) at ZAIKEN, Waseda University.

## APPENDIX A: PARAMETERS OBTAINED BY THE FITTING OF THE PHOTOINDUCED CHANGE IN THE REFLECTIVITY SPECTRA

The parameters obtained by the fitting of the original optical conductivity spectra and the shifted parameters obtained by the fitting of the photoinduced change in the reflectivity spectra are shown in Table I.

## APPENDIX B: THE $T$ DEPENDENCE OF THE PHOTOINDUCED CHANGE IN THE REFLECTIVITY AND ITS ANALYSIS

Figures 7(a)–7(c) show the time ( $t$ ) dependence of the photoinduced  $\Delta R/R$  at  $\hbar\omega = 1.8$  eV with various intensities of a pump pulse  $p$  applied onto the  $ab$  plane with  $E_{\text{pump}} \parallel a$  and  $E_{\text{probe}} \parallel a$  [corresponding to Figs. 5(a) and 5(b) in the main text] in three different ranges of  $t$ . In general, the  $t$  dependence for  $0 < t < 1$  ps is mainly dominated by the excitation with an electronic origin, that for  $1 < t < 100$  ps is dominated by the increase in the temperature of lattice and the strain wave (shock wave), and that for  $100 < t < 5000$  ps is dominated by thermal conduction.

Based on the model shown in Ref. [19], we analyze the  $t$  dependence of  $\Delta R/R$  for  $0 < t < 100$  ps by assuming the following  $z$ - and  $t$ -dependent complex dielectric constant,

$$\begin{aligned} \varepsilon(z, t) &= \varepsilon_\beta + \gamma \Delta\varepsilon \quad (0 \leq z < vt) \\ &= \varepsilon_\beta + \gamma \Delta\varepsilon \exp\left(-\frac{z-vt}{d}\right) \quad (vt \leq z), \end{aligned} \quad (\text{B1})$$

where  $\varepsilon(z, t)$  is the complex dielectric constant at a distance  $z$  from the surface and at time  $t$ .  $\Delta\varepsilon$  is given as

$$\Delta\varepsilon = \varepsilon_\lambda - \varepsilon_\beta, \quad (\text{B2})$$

where  $\varepsilon_\beta$  and  $\varepsilon_\lambda$  are the complex dielectric constants of  $\text{Ti}_3\text{O}_5$  (the  $\beta$  phase) and  $\text{Ti}_{2.75}\text{Al}_{0.25}\text{O}_5$  (the  $\lambda$  phase), respectively, at room temperature at the corresponding value of  $\hbar\omega$  (1.8 eV) in the corresponding direction ( $a$  axis) obtained by the reflectivity measurement. This model assumes that a photoinduced phase (the  $\lambda$  phase) with the thickness of  $d$  appears immediately after the photoirradiation, and it evolves associated with the strain wave that propagates with the sound velocity  $v$ , as illustrated in Fig. 7(d). With this  $\varepsilon(z, t)$ , the reflectivity  $R(t)$  at  $\hbar\omega = 1.8$  eV was calculated.

Dashed lines in Fig. 7(b) are the results of the calculation with  $v$  (sound velocity),  $d$  (the width of the photoinduced phase upon the initial photoirradiation), and  $\gamma$  (ratio of the  $\lambda$  phase in the photoinduced phase) as fitting parameters. The parameters obtained by the fitting are as follows:  $v = 5 \times 10^3$  m/s,  $d = 25$  nm, and  $\gamma = 0.27$  for  $p = 15$  mJ/cm<sup>2</sup>,  $v = 5 \times 10^3$  m/s,  $d = 65$  nm, and  $\gamma = 0.50$  for  $p = 24$  mJ/cm<sup>2</sup>, and  $v = 7 \times 10^3$  m/s,  $d = 200$  nm, and  $\gamma = 1.0$  for  $p = 33$  mJ/cm<sup>2</sup>. A reasonable agreement between the experimental and calculated results indicates that the model above is appropriate to explain the  $t$  dependence of  $\Delta R/R$  for  $0 < t < 100$  ps.

The  $t$  dependence of  $\Delta R/R$  for  $0 < t < 5000$  ps has been analyzed as follows: We assume that the dielectric constant changes in proportion to the change in the temperature  $T$ ,

$$\varepsilon(z, t) = \varepsilon_\beta + \delta\varepsilon(T(z, t) - T_0), \quad (\text{B3})$$

TABLE I. Parameters of the Lorentz functions before the irradiation of a laser pulse ( $\omega_i, \gamma_i, C_i$ ) and  $t = 7$  ps after the irradiation of a laser pulse ( $\omega'_i, \gamma'_i, C'_i$ ) (a) on the  $ac$  plane with  $E_{\text{pump}} \parallel a$  and  $E_{\text{probe}} \parallel c$  with a power density of  $p = 24$  mJ/cm<sup>2</sup> [corresponding to Figs. 3(c) and 3(d) of the main text], (b) on the  $ab$  plane with  $E_{\text{pump}} \parallel a$  and  $E_{\text{probe}} \parallel a$  with a power density of  $p = 33$  mJ/cm<sup>2</sup> [corresponding to Figs. 5(c) and 5(d) of the main text], and (c) on the  $ac$  plane with  $E_{\text{pump}} \parallel a$  and  $E_{\text{probe}} \parallel a$  with a power density of  $p = 24$  mJ/cm<sup>2</sup> [corresponding to Figs. 8(c) and 8(d) in Appendix C].

(a) Figs. 3(c) and 3(d)						
$i$	$\omega_i$ (eV)	$\gamma_i$ (eV)	$C_i$ ( $\Omega^{-1} \text{cm}^{-1}$ eV)	$\omega'_i$ (eV)	$\gamma'_i$ (eV)	$C'_i$ ( $\Omega^{-1} \text{cm}^{-1}$ eV)
1	0.973	1.0	902	0.867	0.97	968
2	1.909	1.15	202	1.878	1.33	168
3	2.744	0.70	76	2.667	0.66	73
4	4.53	1.27	2694			
(b) Figs. 5(c) and 5(d)						
$i$	$\omega_i$ (eV)	$\gamma_i$ (eV)	$C_i$ ( $\Omega^{-1} \text{cm}^{-1}$ eV)	$\omega'_i$ (eV)	$\gamma'_i$ (eV)	$C'_i$ ( $\Omega^{-1} \text{cm}^{-1}$ eV)
1	1.140	1.26	707	1.118	1.15	659
2	1.859	1.08	444	2.074	1.32	374
3	3.055	0.64	123	2.986	0.66	136
4	4.69	1.71	3881			
(c) Figs. 8(c) and 8(d)						
$i$	$\omega_i$ (eV)	$\gamma_i$ (eV)	$C_i$ ( $\Omega^{-1} \text{cm}^{-1}$ eV)	$\omega'_i$ (eV)	$\gamma'_i$ (eV)	$C'_i$ ( $\Omega^{-1} \text{cm}^{-1}$ eV)
1	1.141	0.92	307	1.012	0.71	235
2	1.923	1.02	666	1.721	1.20	677
3	3.433	1.34	822	3.486	2.04	925
4	4.80	1.21	3634			

where  $T(z, t)$  is the temperature at a distance  $z$  from the surface and at time  $t$ ,  $T_0$  is the room temperature, and  $\delta\varepsilon$  is the change in the complex dielectric constant when  $T$  increases by 1 K.  $T(z, t)$  is determined by the thermal conduction equation,

$$\kappa \frac{\partial^2 T(z, t)}{\partial z^2} = c \frac{\partial T(z, t)}{\partial t}, \quad (\text{B4})$$

where  $\kappa$  is the thermal conductivity and  $c$  is the specific heat of the material. The initial condition of the  $T(z, t)$  is assumed to be dominated by the penetration depth of the pump pulse, and is given as

$$T(z, 0) = T_0 + a \exp\left(-\frac{z}{d}\right). \quad (\text{B5})$$

The time evolution of  $\varepsilon(z, t)$  in this model is shown in Fig. 7(e). Note that the free parameters in this model are  $a\delta\varepsilon$  (a complex number),  $\kappa/c$ , and  $d$ .  $d$  is fixed to 60 nm based on the experimentally obtained extinction coefficient at 1.8 eV, and  $c$  is fixed to 3.7 J/cm<sup>3</sup> K, which is the specific heat of rutile  $\text{TiO}_2$ . For  $\delta\varepsilon$ , since  $\varepsilon_1$  (real part) and  $\varepsilon_2$  (imaginary part) of  $\text{Ti}_3\text{O}_5$  at  $\hbar\omega = 1.8$  eV is 3.4 and 3.7, respectively, we took  $\delta\varepsilon$  with the 1 : 1 ratio of the real part and the imaginary part. The dashed line in Fig. 7(c) is the result with  $\kappa = 6$  W/mK and  $a\delta\varepsilon = 0.2 + 0.2i$ .

#### APPENDIX C: PHOTOINDUCED SPECTRA ON THE $ac$ PLANE WITH $E_{\text{pump}} \parallel a$ AND $E_{\text{probe}} \parallel a$

Figure 8 shows the photoinduced  $\Delta R/R$  spectra on the  $ac$  plane with  $E_{\text{pump}} \parallel a$  and  $E_{\text{probe}} \parallel a$  and the analysis of the spectrum, similarly to Fig. 3 and Fig. 5 of the main text.

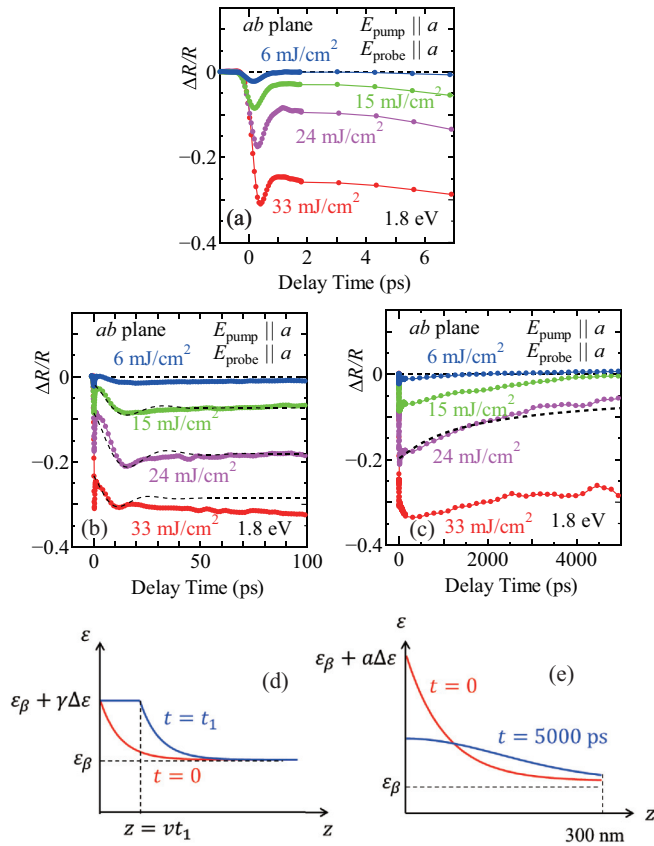


FIG. 7. (a)–(c) Time ( $t$ ) dependence of the photoinduced change in the reflectivity  $\Delta R/R$  on the *ab* plane with  $E_{\text{pump}} \parallel a$  and  $E_{\text{probe}} \parallel a$  (corresponding to Fig. 5 of the main text) with various power densities  $p$  for (a)  $0 \leq t \leq 7$  ps, (b)  $0 \leq t \leq 100$  ps, and (c)  $0 \leq t \leq 5000$  ps. (d), (e) Schematics of the position ( $z$ ) dependence of the dielectric constant  $\epsilon(z)$  at various times  $t$  used for the analysis of  $\Delta R/R$  for (d)  $0 \leq t \leq 100$  ps and (e)  $0 \leq t \leq 5000$  ps.

Comparison of these results indicate that the photoinduced change on the *ac* plane with  $E_{\text{pump}} \parallel a$  and  $E_{\text{probe}} \parallel a$  shown in Fig. 8 is dominated by the shift of the peak frequencies  $\omega_i$  to lower values. This is similar to the spectral change on the *ac* plane with  $E_{\text{pump}} \parallel a$  and  $E_{\text{probe}} \parallel c$  shown in Fig. 3 of the main text, but quite different from the spectral change on the *ab* plane with  $E_{\text{pump}} \parallel a$  and  $E_{\text{probe}} \parallel a$  shown in Fig. 5, where it is dominated by the suppression of the spectral weight for the peak at  $\sim 2.0$  eV.

The difference between the original  $\sigma(\omega)$  spectrum along the *a* axis in Fig. 5(c) and that in Fig. 8(c) arises from the fact that the spectrum in Fig. 5 is measured on the polished surface along the *ab* plane whereas that in Fig. 8 is measured on the cleaved surface along the *ac* plane.

#### APPENDIX D: EFFECT OF POLISHING ON THE PHOTOINDUCED SPECTRA

To see whether the polishing of the sample surface can affect the photoinduced spectra, we performed the pump-probe measurement of  $\text{Ti}_3\text{O}_5$  both on the cleaved surface and the polished surface along the *ac* plane with  $E_{\text{pump}} \parallel a$  and  $E_{\text{probe}} \parallel a$ . Figure 9 shows the photoinduced change in the

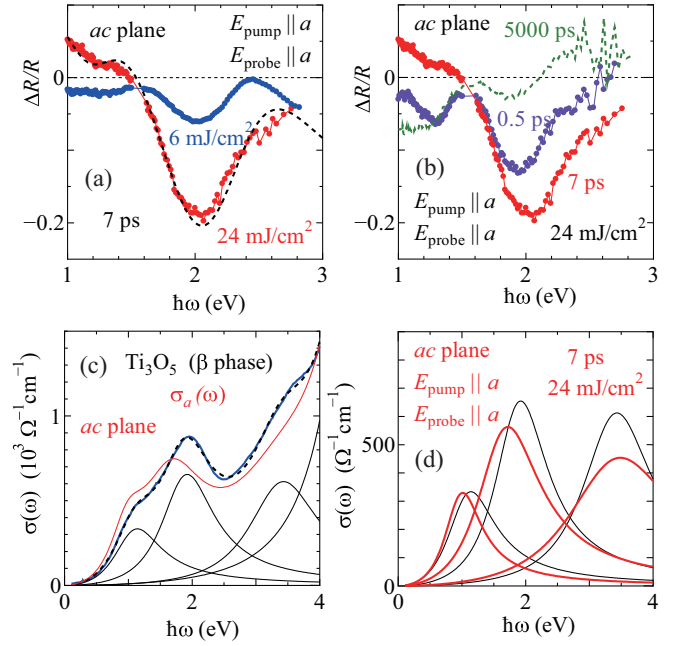


FIG. 8. (a), (b) Photoinduced change in the reflectivity spectra  $\Delta R/R$  on the *ac* plane with  $E_{\text{pump}} \parallel a$  and  $E_{\text{probe}} \parallel a$  at (a)  $t = 7$  ps after a pump pulse with a power density of  $p = 6$  or  $24$   $\text{mJ}/\text{cm}^2$  is applied and (b)  $t = 0.5, 7$ , and  $5000$  ps after a pump pulse with  $p = 24$   $\text{mJ}/\text{cm}^2$  is applied. The dashed line in (a) is a fitting curve (see text). (c) Decomposition of the optical conductivity spectrum of  $\text{Ti}_3\text{O}_5$  along the *a* axis into four Lorentz functions. The dashed line is the sum of the Lorentz functions, and the red solid line is the sum of the Lorentz functions with shifted parameters for the photoinduced spectrum in (d). (d) Three Lorentz functions for the optical conductivity spectrum along the *a* axis on the *ac* plane before the application of a pump pulse (thin black lines) and at  $7$  ps after a pump pulse of  $24$   $\text{mJ}/\text{cm}^2$  is applied (thick red lines).

reflectivity spectra  $\Delta R/R$  at  $7$  ps after a pump pulse with a power density of (a)  $p = 6$  or  $24$   $\text{mJ}/\text{cm}^2$  is applied on the cleaved surface and (b) that of  $p = 15$  or  $33$   $\text{mJ}/\text{cm}^2$  is applied on the polished surface. As can be seen, the  $\Delta R/R$  spectra are barely different, indicating that polishing barely affects the photoinduced phase transition.

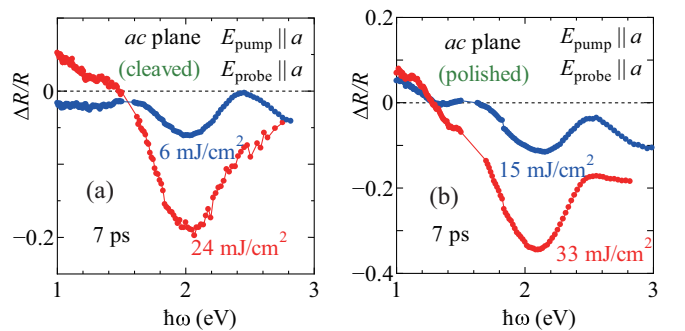


FIG. 9. (a), (b) Photoinduced change in the reflectivity spectra  $\Delta R/R$  with  $E_{\text{pump}} \parallel a$  and  $E_{\text{probe}} \parallel a$  at  $t = 7$  ps after (a) a pump pulse with a power density of  $p = 6$  or  $24$   $\text{mJ}/\text{cm}^2$  is applied on the cleaved surface along the *ac* plane and (b) that of  $p = 15$  or  $33$   $\text{mJ}/\text{cm}^2$  is applied on the polished surface along the *ac* plane.



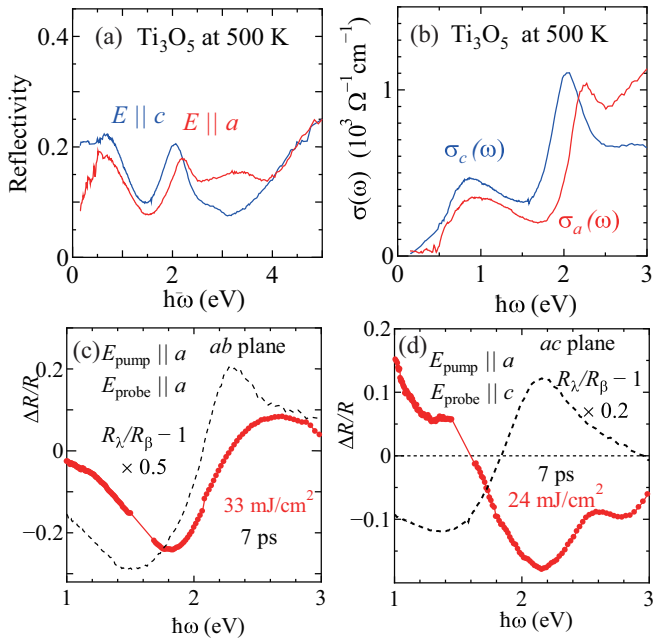


FIG. 10. (a) Reflectivity and (b) optical conductivity spectra along the  $ac$  plane with  $E \parallel a$  and  $c$  for  $\text{Ti}_3\text{O}_5$  at 500 K. (c), (d) Photoinduced changes in the reflectivity spectra  $\Delta R/R$  at  $t = 7$  ps for (c)  $E_{\text{pump}} \parallel a$  and  $E_{\text{probe}} \parallel a$  with  $p = 33$   $\text{mJ}/\text{cm}^2$  on the  $ab$  plane and (d)  $E_{\text{pump}} \parallel a$  and  $E_{\text{probe}} \parallel c$  with  $p = 24$   $\text{mJ}/\text{cm}^2$  on the  $ac$  plane (solid circles and lines). Dashed lines in (c) and (d) show the difference between the reflectivity spectrum of  $\text{Ti}_3\text{O}_5$  at 500 K and that at room temperature with a corresponding polarization of the probe pulse.

#### APPENDIX E: REFLECTIVITY SPECTRA OF $\text{Ti}_3\text{O}_5$ AT HIGH TEMPERATURES

We made an attempt to measure the reflectivity of  $\text{Ti}_3\text{O}_5$  in the IT phase ( $\lambda$  phase). Figure 10(a) shows the reflectivity spectra for  $\text{Ti}_3\text{O}_5$  with  $E \parallel a$  and  $E \parallel c$  on a cleaved surface along the  $ac$  plane at 500 K, and Fig. 10(b) shows the optical conductivity spectra  $\sigma_a(\omega)$  and  $\sigma_c(\omega)$  obtained by the Kramers-Kronig transformation of the reflectivity spectra. As can be seen, the reflectivity spectra and the optical conductivity spectra at 500 K are discernibly different from those

for  $\text{Ti}_3\text{O}_5$  at room temperature shown in Figs. 2(a) and 2(c). However, they are also different from those for  $\text{Ti}_{2.75}\text{Al}_{0.25}\text{O}_5$  at room temperature shown in Figs. 2(b) and 2(d), which is also in the  $\lambda$  phase. Both  $\sigma_a(\omega)$  and  $\sigma_c(\omega)$  for  $\text{Ti}_3\text{O}_5$  at 500 K have a broad peak around 1 eV [Fig. 10(b)], similarly to those for  $\text{Ti}_{2.75}\text{Al}_{0.25}\text{O}_5$  at room temperature [Fig. 2(d)], but there is a sharp peak at 2.2 ~ 2.3 eV both in  $\sigma_a(\omega)$  and  $\sigma_c(\omega)$  for  $\text{Ti}_3\text{O}_5$  at 500 K [Fig. 10(b)], but it is absent both in  $\sigma_a(\omega)$  and  $\sigma_c(\omega)$  for  $\text{Ti}_{2.75}\text{Al}_{0.25}\text{O}_5$  at room temperature [Fig. 2(d)].

As the origin of this discrepancy, we speculate that the surface of  $\text{Ti}_3\text{O}_5$  at 500 K is not fully in the  $\lambda$  phase but the  $\beta$  and  $\lambda$  phases coexist at the surface. This may be due to the residual stress near the sample surface and also due to the fact that 500 K is too close to the phase boundary, though we cannot increase the temperature higher than 500 K owing to the limitation of the apparatus. Such two-phase coexisting may result in the anomalous reflectivity spectra for  $\text{Ti}_3\text{O}_5$  [41].

We compare in Fig. 10(c) the photoinduced reflectivity change  $\Delta R/R$  for  $\text{Ti}_3\text{O}_5$  along the  $ab$  plane of  $\text{Ti}_3\text{O}_5$  with  $E_{\text{pump}} \parallel a$  at  $t = 7$  ps with  $p = 33$   $\text{mJ}/\text{cm}^2$  [shown in Figs. 5(a), 5(b) and 6(b)] with the difference between the reflectivity spectra for  $\text{Ti}_3\text{O}_5$  with  $E \parallel a$  at 500 K and that at 300 K. Although the similarity between the two spectra is not as impressive as the similarity between the photoinduced change and the difference spectra of  $\text{Ti}_3\text{O}_5$  and  $\text{Ti}_{2.75}\text{Al}_{0.25}\text{O}_5$  shown in Fig. 6(b), the overall trend of the two spectra is quite similar, indicating that a photoinduced phase transition occurs in this configuration.

We also compare in Fig. 10(d) the photoinduced reflectivity change  $\Delta R/R$  for  $\text{Ti}_3\text{O}_5$  along the  $ac$  plane with  $E_{\text{pump}} \parallel c$  at  $t = 7$  ps with  $p = 24$   $\text{mJ}/\text{cm}^2$  [shown in Figs. 3(a), 3(b) and 6(c)] with the difference between the reflectivity spectra for  $\text{Ti}_3\text{O}_5$  with  $E \parallel c$  at 500 K and that at 300 K. As can be seen, they are quite different, the same situation as the comparison between the photoinduced change and the difference spectra of  $\text{Ti}_3\text{O}_5$  and  $\text{Ti}_{2.75}\text{Al}_{0.25}\text{O}_5$  shown in Fig. 6(c), indicating that a photoinduced phase transition does not occur in this configuration. Therefore, using the spectrum of  $\text{Ti}_3\text{O}_5$  at 500 K instead of  $\text{Ti}_{2.75}\text{Al}_{0.25}\text{O}_5$  at room temperature as the spectrum of the  $\lambda$  phase does not change the conclusion of the present paper.

- [1] M. F. Becker, A. B. Buckman, R. M. Walsler, T. Lépine, P. Georges, and A. Brun, Femtosecond laser excitation of the semiconductor-metal phase transition in  $\text{VO}_2$ , *Appl. Phys. Lett.* **65**, 1507 (1994).
- [2] A. Cavalleri, C. Tóth, C. W. Siders, J. A. Squier, F. Rákai, P. Forget, and J. C. Kieffer, Femtosecond Structural Dynamics in  $\text{VO}_2$  during an Ultrafast Solid-Solid Phase Transition, *Phys. Rev. Lett.* **87**, 237401 (2001).
- [3] S. Iwai, M. Ono, A. Maeda, H. Matsuzaki, H. Kishida, H. Okamoto, and Y. Tokura, Ultrafast Optical Switching to a Metallic State by Photoinduced Mott Transition in a Halogen-Bridged Nickel-Chain Compound, *Phys. Rev. Lett.* **91**, 057401 (2003).
- [4] S. Iwai and H. Okamoto, Ultrafast phase control in one-dimensional correlated electron systems, *J. Phys. Soc. Jpn.* **75**, 011007 (2006).
- [5] H. Okamoto, H. Matsuzaki, T. Wakabayashi, Y. Takahashi, and T. Hasegawa, Photoinduced Metallic State Mediated by Spin-Charge Separation in a One-Dimensional Organic Mott Insulator, *Phys. Rev. Lett.* **98**, 037401 (2007).
- [6] H. Okamoto, T. Miyagoe, K. Kobayashi, H. Uemura, H. Nishioka, H. Matsuzaki, A. Sawa, and Y. Tokura, Ultrafast charge dynamics in photoexcited  $\text{Nd}_2\text{CuO}_4$  and  $\text{La}_2\text{CuO}_4$  cuprate compounds investigated by femtosecond absorption spectroscopy, *Phys. Rev. B* **82**, 060513(R) (2010).
- [7] S. Wall, D. Brida, S. R. Clark, H. P. Ehrke, D. Jaksch, A. Ardavan, S. Bonora, H. Uemura, Y. Takahashi, T. Hasegawa, H. Okamoto, G. Cerullo, and A. Cavalleri, Quantum interference between charge excitation paths in a solid-state Mott insulator, *Nat. Phys.* **7**, 114 (2011).
- [8] M. Liu, H. Y. Hwang, H. Tao, A. C. Strikwerda, K. Fan, G. R. Keiser, A. J. Sternbach, K. G. West, S. Kittiwatanakul, J. Lu,

- S. A. Wolf, F. G. Omenetto, X. Zhang, K. A. Nelson, and R. D. Averitt, Terahertz-field-induced insulator-to-metal transition in vanadium dioxide metamaterial, *Nature (London)* **487**, 345 (2012).
- [9] F. Novelli, D. Fausti, J. Reul, F. Cilento, P. H. M. van Loosdrecht, A. A. Nugroho, T. T. M. Palstra, M. Grüninger, and F. Parmigiani, Ultrafast optical spectroscopy of the lowest energy excitations in the Mott insulator compound  $\text{YVO}_3$ : Evidence for Hubbard-type excitons, *Phys. Rev. B* **86**, 165135 (2012).
- [10] H. Yamakawa, T. Miyamoto, T. Morimoto, T. Terashige, H. Yada, N. Kida, M. Suda, H. M. Yamamoto, R. Kato, K. Miyagawa, K. Kanoda, and H. Okamoto, Mott transition by an impulsive dielectric breakdown, *Nat. Mater.* **16**, 1100 (2017).
- [11] M. Chollet, L. Guerin, N. Uchida, S. Fukaya, H. Shimoda, T. Ishikawa, K. Matsuda, T. Hasegawa, A. Ota, H. Yamochi, G. Saito, R. Tazaki, S.-i. Adachi, and S.-y. Koshihara, Gigantic photoresponse in 1/4-filled-band organic salt  $(\text{EDO-TTF})_2\text{PF}_6$ , *Science* **307**, 86 (2005).
- [12] Y. Kawakami, T. Fukatsu, Y. Sakurai, H. Unno, H. Itoh, S. Iwai, T. Sasaki, K. Yamamoto, K. Yakushi, and K. Yonemitsu, Early-Stage Dynamics of Light-Matter Interaction Leading to the Insulator-to-Metal Transition in a Charge Ordered Organic Crystal, *Phys. Rev. Lett.* **105**, 246402 (2010).
- [13] H. Ichikawa, S. Nozawa, T. Sato, A. Tomita, K. Ichiyangi, M. Chollet, L. Guerin, N. Dean, A. Cavalleri, S.-i. Adachi, T.-h. Arima, H. Sawa, Y. Ogimoto, M. Nakamura, R. Tamaki, K. Miyano, and S.-y. Koshihara, Transient photoinduced ‘hidden’ phase in a manganite, *Nat. Mater.* **10**, 101 (2011).
- [14] T. Ishikawa, Y. Sagae, Y. Naitoh, Y. Kawakami, H. Itoh, K. Yamamoto, K. Yakushi, H. Kishida, T. Sasaki, S. Ishihara, Y. Tanaka, K. Yonemitsu, and S. Iwai, Optical freezing of charge motion in an organic conductor, *Nat. Commun.* **5**, 5528 (2014).
- [15] M. Rini, R. Tobey, N. Dean, J. Itatani, Y. Tomioka, Y. Tokura, R. W. Schoenlein, and A. Cavalleri, Control of the electronic phase of a manganite by mode-selective vibrational excitation, *Nature (London)* **449**, 72 (2007).
- [16] D. A. Mazurenko, A. A. Nugroho, T. T. M. Palstra, and P. H. M. van Loosdrecht, Dynamics of Spin and Orbital Phase Transitions in  $\text{YVO}_3$ , *Phys. Rev. Lett.* **101**, 245702 (2008).
- [17] K. Takubo, Y. Onishi, A. Furuhashi, A. Nogami, and T. Katsufuji, Photoinduced dynamics of spinel  $\text{MnV}_2\text{O}_4$ , *Phys. Rev. B* **88**, 214416 (2013).
- [18] O. Sato, T. Iyoda, A. Fujishima, and K. Hashimoto, Photoinduced magnetization of a cobalt-iron cyanide, *Science* **272**, 704 (1996).
- [19] Y. Okimoto, X. Peng, M. Tamura, T. Morita, K. Onda, T. Ishikawa, S. Koshihara, N. Todoroki, T. Kyomen, and M. Itoh, Ultrasonic Propagation of a Metallic Domain in  $\text{Pr}_{0.5}\text{Ca}_{0.5}\text{CoO}_3$  Undergoing a Photoinduced Insulator-Metal Transition, *Phys. Rev. Lett.* **103**, 027402 (2009).
- [20] A. Tomeljak, H. Schäfer, D. Städter, M. Beyer, K. Biljakovic, and J. Demsar, Dynamics of Photoinduced Charge-Density-Wave to Metal Phase Transition in  $\text{K}_{0.3}\text{MoO}_3$ , *Phys. Rev. Lett.* **102**, 066404 (2009).
- [21] S. Åsbrink and A. Magnéri, Crystal structure studies on trititanium pentoxide,  $\text{Ti}_3\text{O}_5$ , *Acta Crystallogr.* **12**, 575 (1959).
- [22] L. N. Mulay and W. J. Danley, Cooperative magnetic transitions in the titanium-oxygen system: A new approach, *J. Appl. Phys.* **41**, 877 (1970).
- [23] S.-H. Hong and S. Åsbrink, The structure of  $\gamma\text{-Ti}_3\text{O}_5$  at 297 K, *Acta Crystallogr., Sect. B* **38**, 2570 (1982).
- [24] M. Onoda, Phase transitions of  $\text{Ti}_3\text{O}_5$ , *J. Solid State Chem.* **136**, 67 (1998).
- [25] S.-i. Ohkoshi, Y. Tsunobuchi, T. Matsuda, K. Hashimoto, A. Namai, F. Hakoe, and H. Tokoro, Synthesis of a metal oxide with a room-temperature photoreversible phase transition, *Nat. Chem.* **2**, 539 (2010).
- [26] A. Asahara, H. Watanabe, H. Tokoro, S.-i. Ohkoshi, and T. Suemoto, Ultrafast dynamics of photoinduced semiconductor-to-metal transition in the optical switching nano-oxide  $\text{Ti}_3\text{O}_5$ , *Phys. Rev. B* **90**, 014303 (2014).
- [27] K. Tanaka, T. Nasu, Y. Miyamoto, N. Ozaki, S. Tanaka, T. Nagata, F. Hakoe, M. Yoshikiyo, K. Nakagawa, Y. Umetsu, K. Imoto, H. Tokoro, A. Namai, and S.-i. Ohkoshi, Structural phase transition between  $\gamma\text{-Ti}_3\text{O}_5$  and  $\delta\text{-Ti}_3\text{O}_5$  by breaking of a one-dimensionally conducting pathway, *Cryst. Growth Design* **15**, 653 (2015).
- [28] K. Yoshimatsu, O. Sakata, and A. Ohtomo, Superconductivity in  $\text{Ti}_4\text{O}_7$  and  $\gamma\text{-Ti}_3\text{O}_5$  films, *Sci. Rep.* **7**, 12544 (2017).
- [29] R. Takahama, T. Ishii, D. Indo, M. Arizono, C. Terakura, Y. Tokura, N. Takeshita, M. Noda, H. Kuwahara, T. Saiki, T. Katsufuji, R. Kajimoto, and T. Okuda, Structural, magnetic, transport, and thermoelectric properties of the pseudobrookite  $\text{AlTi}_2\text{O}_5\text{-Ti}_3\text{O}_5$  system, *Phys. Rev. Mater.* **4**, 074401 (2020).
- [30] H. Chen, Y. Hirose, K. Nakagawa, K. Imoto, S.-i. Ohkoshi, and T. Hasegawa, Non-metallic electrical transport properties of a metastable  $\lambda\text{-Ti}_3\text{O}_5$  thin film epitaxially stabilized on a pseudobrookite seed layer, *Appl. Phys. Lett.* **116**, 201904 (2020).
- [31] C. Mariette, M. Lorenc, H. Cailleau, E. Collet, L. Guérin, A. Volte, E. Trzop, R. Bertoni, X. Dong, B. Lépine, O. Hernandez, E. Janod, L. Cario, V. Ta Phuoc, S. Ohkoshi, H. Tokoro, L. Patthey, A. Babic, I. Ussov, D. Ozerov, L. Sala *et al.*, Strain wave pathway to semiconductor-to-metal transition revealed by time-resolved x-ray powder diffraction, *Nat. Commun.* **12**, 1239 (2021).
- [32] K. Momma and F. Izumi, VESTA3 for three-dimensional visualization of crystal, volumetric and morphology data, *J. Appl. Crystallogr.* **44**, 1272 (2011).
- [33] S.-y. Koshihara and S.-i. Adachi, Photo-induced phase transition in an electron-lattice correlated system: Future role of a time-resolved x-ray measurement for materials science, *J. Phys. Soc. Jpn.* **75**, 011005 (2006).
- [34] N. F. Brady, K. Appavoo, M. Seo, J. Nag, R. P. Prasankumar, R. F. Haglund, and D. J. Hilton, Heterogeneous nucleation and growth dynamics in the light-induced phase transition in vanadium dioxide, *J. Phys.: Condens. Matter* **28**, 125603 (2016).
- [35] Z. Tao, F. Zhou, T.-R. T. Han, D. Torres, T. Wang, N. Sepulveda, K. Chang, M. Young, R. R. Lunt, and C.-Y. Ruan, The nature of photoinduced phase transition and metastable states in vanadium dioxide, *Sci. Rep.* **6**, 38514 (2016).
- [36] F. Randi, I. Vergara, F. Novelli, M. Esposito, M. Dell’Angela, V. A. M. Brabers, P. Metcalf, R. Kukreja, H. A. Dürr, D. Fausti, M. Grüninger, and F. Parmigiani, Phase separation in the nonequilibrium Verwey transition in magnetite, *Phys. Rev. B* **93**, 054305 (2016).
- [37] Y. Toyozawa, *Optical Processes in Solids* (Cambridge University Press, London, 2003).

- [38] C. Thomsen, H. T. Grahn, H. J. Maris, and J. Tauc, Surface generation and detection of phonons by picosecond light pulses, *Phys. Rev. B* **34**, 4129 (1986).
- [39] C. Rose-Petruck, R. Jimenez, T. Guo, A. Cavalleri, C. W. Siders, F. Rksi, J. A. Squier, B. C. Walker, K. R. Wilson, and C. P. J. Barty, Picosecond-milliångström lattice dynamics measured by ultrafast x-ray diffraction, *Nature (London)* **398**, 310 (1999).
- [40] S. O. Mariager, F. Pressacco, G. Ingold, A. Caviezel, E. Möhr-Vorobeva, P. Beaud, S. L. Johnson, C. J. Milne, E. Mancini, S. Moyerman, E. E. Fullerton, R. Feidenhans'l, C. H. Back, and C. Quitmann, Structural and Magnetic Dynamics of a Laser Induced Phase Transition in FeRh, *Phys. Rev. Lett.* **108**, 087201 (2012).
- [41] Since the Kramers-Kronig transformation from reflectivity to optical conductivity is not a linear transformation, the optical conductivity spectrum obtained by the reflectivity spectrum of a two-phase-coexisting sample is not a simple superposition of the two spectra.